Iranian Journal of Electrical and Electronic Engineering

Journal Homepage: ijeee.iust.ac.ir

Image Fusion using Bio-Inspired Neural P Systems and Non-Subsampled Shearlet Transform for Improved Diagnosis of Brain Tumors

Dr. Ch. Suryababu*(C.A), B. Vijaya**, Dr. Arempula Sreenivasa Rao***, G.Sattibabu****, Dr.R.Rambabu*****, Dr. K. Ravi Kumar******

Abstract: Diagnostic image fusion across multiple modalities integrates diverse images, making it a crucial tool for improved diagnosis. To achieve the best fusion outcomes between MRI and PET brain images, the study presents an enhanced image fusion strategy that combines Spiking Neural P Systems with Non-subsampled Shearlet Transform (NSST). The proposed system first decomposes images into low-frequency and high-frequency regions by applying NSST and employs dynamic threshold neural P (DTNP) systems for high-frequency fusion and Coupled Neural P (CNP) systems for low-frequency fusion. Through practical testing of 48 pairs of PET and MRI related to various disorders of the brain, it is demonstrated that the suggested strategy outperforms seven popular fusion techniques, such as neuro-fuzzy and CNN-based models. It provides an Improvement in Structural Similarity Index (SSIM) and entropy by 23.8%, 17.6% respectively, compared to existing methods. Our approach helps medical practitioners make better decisions by producing precise observations about brain tumors, neurodegenerative disorders, and Alzheimer's disease. This contemporary fusion technique enhances the clinical interpretation and noticeable quality of fused images, leading to improved medical imaging capabilities.

Keywords: image fusion, Spiking Neural P System, Non-subsampled Shearlet Transform, Coupled Neural P, dynamic threshold neural P, brain tumors, neurodegenerative disorders, Alzheimer's disease

* Professor, Department of ECE, Rajamahendri Institute of Engineering and Technology, Andhra Pradesh, India.
E-mail: suryajessica@gmail.com
** Assistant Professor, Department of ECE, PACE Institute of Technology and Sciences, Andhra Pradesh, India.
E-mail: vijaya29329@gmail.com
*** Associate Professor, Department of ECE, Annamacharya Institute of Technology and Sciences, Telangana, India
E-mail: asraoecehod@gmail.com
**** Assistant Professor, Department of ECE, Aditya University, Surampalem, Andhra Pradesh, India
E-mail: satish.babu2007@gmail.com
***** Professor, Department of CSE, Rajamahendri Institute of Engineering and Technology, Andhra Pradesh, India
E-mail: rambabureddy.rampatruni@gmail.com
****** Professor, Department of ECE, Avanthi Institute of Engineering and Technology, Andhra Pradesh, India
E-mail: ravikumarkolakaluri@gmail.com
Corresponding author:Dr. Ch. Suryababu

1. Introduction

The technique of fusing data from multiple independent data sources to create an improved version of information that allows for qualitative inference is known as fusion. Image fusion is frequently used in industrial applications, medical imaging, remote sensing, and many other applications. Medical imaging is complicated and requires a variety of modalities to obtain all the information required for a particular body tissue. Images of excellent quality are produced using image fusion. However, hyperspectral, multispectral, and high dynamic range images are also capable of producing optimal quality images. Clinical diagnosis requires medical imaging because a thorough understanding of

anatomical and functional aspects enables accurate diagnosis. In medical applications, each of the clinical imaging techniques—MRI, PET, CT, and SPECT has unique disadvantages [1-2].

Although MRI does not provide functional diagnostic capabilities, its primary strength is its high spatial clarity, whereas PET and SPECT provide functional diagnostic data with lower degrees of spatial resolution. In medical diagnostics, image fusion operations combine different imaging modalities to obtain better diagnostic data. Pixel-based, feature-based, and decision-based fusion are some of the different techniques used to fuse images. Conventional fusion procedures that use averaging, maximum, and minimum techniques are unable to adequately retain basic tissue properties and texture elements. The inability of feature-based methods to deal with noise and misalignment between identified features is comparable to their drawbacks. Although several fusion techniques are used, decision-based fusion solutions require extensive parameter adjustment. As a result of their ability to obtain information at various scales and orientations, Wavelet Transform (WT) and Non-subsampled Shearlet Transform (NSST) have become prominent transform domain fusion approaches. The present work proposes a novel multimodal medical image fusion system that primarily uses coupled neural P and dynamic threshold neural P systems (CNP-DTNP) along with NSST.

Despite significant advancements in CNN-driven, wavelet-based, and sparse-representation fusion frameworks, current approaches have drawbacks such as the inability to manage localized fluctuations in multimodal inputs, the loss of structural information, or reliance on large training datasets. While traditional NSST or PCNN algorithms find it difficult to strike a compromise between edge sharpness and noise reduction, CNN-based models perform poorly when data shortage occurs. The proposed NSST–CNP–DTNP framework was developed in response to these deficiencies. It uses dynamic thresholding and localized spike-driven processing to accomplish structure-preserving, training-free fusion.

1.1 Novel Framework of Fusion

The suggested NSST-CNP-DTNP hybrid fusion method enables medical practitioners to preserve crucial diagnostic information by effectively combining frequency-domain and spatial domain medical imaging data. A potential remedy for low-frequency and high-frequency fusion operations is offered by the coupled neural P systems (CNP) and the dynamic threshold neural P system (DTNP). In contrast to traditional average-based fusion, a neural P fusion platform maximizes diagnostic accuracy by preserving structural precision and minimizing information degradation through its mechanism, which ideally integrates low-frequency and high-frequency components.

1.2 Performance Assessment on Authentic Medical Datasets

The suggested technique is evaluated using 48 pairs of PET and MRI brain scans, covering Caudate Head, Caudate Body, Calcarine Fissure, Anterior Cingulate, Amygdala, and Angular Gyrus.

1.3 Superior Objective and Subjective Results

Experiments demonstrate that the suggested strategy works better than seven cutting-edge fusion techniques, including Neuro-Fuzzy and CNN-based systems, Adaptive PCNN, and Laplacian Filtering methods.

1. Improved Structural Similarity Index (SSIM) by 23.8% revealing preservation of structural content of source images in the fused image.

2. Improved Entropy by 17.6% revealing a high amount of texture and information transfer from source images into the fused image.

A larger standard deviation value maintains information density while enabling significant improvements in contrast and detail retention.

1.4 Improved Interpretability in Clinical Settings

The clear visual results produced by this proposed fusion technique assist medical staff in examining conditions, including Alzheimer's disease, neurological diseases, and brain cancers. By integrating transform domain fusion techniques with spiking neural computing, this work improves clinical diagnosis and helps healthcare settings make better therapeutic decisions. Testing is done using co-aligned pairs of MRI & CT, PET & MRI, and MRI & SPECT image pairs from the Harvard Medical Image Fusion Datasets. These publicly available datasets continue to be among the most frequently utilized tools in medical image fusion studies. Throughout the examination, 48 pairs of PET and MRI images are used, with an emphasis on various medical disorders and multiform anatomical structures.

Spiking Neural P Systems provide event-driven computation, which only stimulates neurons when membrane potentials surpass a dynamic threshold, in contrast to traditional neural networks and fuzzy-logic-based fusion frameworks. Because local spatial variations must be accurately captured without superfluous processing, SNP systems are naturally suited for image fusion. Compared to conventional ANN and fuzzy logic systems, its localized communication, spike-based modeling, and dynamic thresholding provide better noise suppression, greater edge retention, and increased sensitivity to pixel-level intensity fluctuations. These

features make it possible for the CNP and DTNP models to more successfully maintain functional details from PET and structural information from MRI.

2. Literature Review

In recent years, a number of fusion techniques for multimodal medical imaging have been introduced. Singh and Khare [3] introduced a multi-modality medical image fusion method that fused the complex wavelet coefficients of source images by applying the Daubechies complex wavelet transform and the maximum criteria of selection. A fusion technique to process multi-modality medical images was studied by Singh and Anand [4] using both the characteristics obtained by the pulse coupled neural network and the discrete ripplet transform (DRT). Relying on the multiscale geometric assessment of the contourlet transform, Yang et al. [5] proposed a method for fusing medical images.
Numerous SR-based fusion techniques have been studied recently [6-7]. However, the SR-based approaches only use one dictionary. Dictionary learning is being included in SR-based techniques to overcome this constraint[8-9]. A discriminatory low-rank sparse dictionary learning-based approach for medical picture fusion was presented by Li et al. [10]. Hu et al. [11] introduced a medical picture fusion technique that relies on Gabor filtering and split dictionary learning. To improve fused images, a novel multi-modal fusion strategy was presented to effectively leverage the morphological diversity aspects of the images and the advantages of morphological component analysis[12].

In their study on pixel convolutional neural networks (CNNs) for multi-focus picture fusion, Tang et al. [13] trained a model to determine the likelihoods of the defocused, focused, and unknown pixels using information about nearby pixels. A CNN-based multi-focus image fusion technique in conjunction with ensemble learning was introduced by Amin-Naji et al. [14]. Typically, these fusion techniques take longer to learn than earlier fusion techniques. A broad multi-modality image fusion framework termed IFCNN was introduced by Zhang et al. [15] employing CNNs. Competitive fusion efficacy has been shown by these DL-based fusion techniques. Li et al. [16] introduced MDLatLRR, a multi-level image decomposition method utilizing latent low-rank encoding.

Attention-driven, transformer-based, and convolution-sparse NSST-domain techniques have been developed in recent developments in multimodal medical image fusion. Improved NSST-based fusion employing sparse representation and local extrema analysis was shown by Guo et al. [17] and Diwakar et al. [18]. Although they have further improved structural retention, transformer-driven fusion networks like M4FNet [19], TCGAN [20], and DesTrans [21] demand a lot of processing power and training. Although they still depend on big datasets, lightweight attention-based models like AMMNet [22] also demonstrate encouraging outcomes. The necessity for effective, training-free substitutes, like the suggested NSST–CNP–DTNP model, which maintains functional as well as structural information without the heavy computational load of deep learning based methods, is reinforced by this research.

From the review of literature, it is evident that Wavelet and transform-based techniques offer strong multi-scale representations, but they have trouble maintaining fine texture variation. Although they require computationally costly tuning, sparse and dictionary-learning techniques enhance detail representation. State-of-the-art fusion is achieved by recent CNN and Transformer-based models, but they need big datasets, a lot of training time, and a lot of memory. On the other hand, the suggested NSST–CNP–DTNP method makes use of training-free, event-driven neural P systems that integrate dynamic thresholding with NSST's directional representation to produce reliable, scalable fusion without the overhead of deep learning.

3. Preliminaries

3.1 Spiking Neural Network Model

Artificial neural networks of the second generation are completely networked and capable of processing control signals and continuous inputs. Spiking neural networks are an improved type of neural network that closely resembles natural neural networks. Artificial neural networks typically communicate information from each neuron after each propagation cycle. This typically occurs at regular periods. Spiking neural networks use membrane charge to transfer information from neurons. When the charge of the membrane reaches a certain value, the transition occurs. This value is referred to as the 'threshold'. Neurons activate when the membrane reaches a threshold. A neuron may acquire or lose energy when it fires.

In the architecture of a spiking neural network, the neurons and synapses are distinguished by their variable weights. Schemes similar to temporal coding are used to transform the analog inputs into the appropriate spikes. Spiking neural networks have far simpler dynamics than biological neural networks. This occurs as a result of the neuron only firing in response to a single parameter, namely the threshold. This stands in contrast to the characteristics of post-inhibitory rebound, refractoriness, resonance dynamics, or hysteresis. The presynaptic neuron mechanism influences the membrane charge of postsynaptic neurons once it reaches a threshold. In either spiking or non-spiking artificial neural networks, the primary source of learning is altering the scalar-valued synaptic weights. Specifically, spiking makes it possible to replicate the bio-plausible learning notion. Non-spiking neural networks do not

permit this type of learning method. The primary goal is to change the weights of the pre- and post-synaptic neurons in milliseconds. Two-layered feed-forward architecture is used in the spiking neural network, with surrounding connections hidden in the second layer.

3.2 Dynamic Threshold Neural P (DTNP) system

A class of collaborative computational models known as DTNP systems [23] is a variant of spiking neural P systems (SNP systems) that incorporates the dynamic threshold and spiking neural mechanism. DTNP systems are conceived of as a matrix of neurons having local connections to carry out the integration of multimodal medical pictures. Assume that P is an M × N medical image and that enhanced novel sum-modified Laplacian, $ENSML_{M\times N}$ is a matrix containing features that reflect the sharp intensity variation components of an image. As a result, a DTNP system is constructed as a matrix of $M \times N$ neurons, as illustrated in figure 1, in which, feature $ENSML_{mn}$ is an external stimuli of neuron σ_{mn} which has a local connection with the neurons in its k -neighborhood $\delta_k(\sigma_{mn}) = \{\sigma_{ij} \mid |i-m| \leq k,\ |j-n| \leq k\ \},\ 1 \leq m \leq M,\ 1 \leq n \leq N$. After implementing the firing rule, neuron σij gets the spikes from its neighboring neurons in δr and then delivers the produced spikes to its neighboring neurons.

The data unit and dynamic threshold unit of neuron σ_{mn} are $[u_{mn}, \tau_{mn}]$, and the spiking rule is $E/(a^u, a^\tau) \rightarrow a^I$. Additionally, each neuron σ_{mn} is both an output neuron as well as an input neuron that receives an external input $ENSML_{mn}$ (i.e., the ENSML score of the NSST coefficients of high-frequency bands at location (m,n)). The firing criterion E for spiking rule $E/(a^u, a^\tau) \rightarrow a^I$ in neuron σ_{mn} is $E = (u_{mn}(t) \geq \tau_{mn}(t)) \wedge (u_{mn}(t) \geq u) \wedge (\tau_{mn}(t) \geq \tau)$. A σ_{mn}neuron fires when the firing criterion is met, signifying that the threshold with value τ in the dynamic threshold unit and the spikes with value u in the data unit are utilized. After that, the neighboring neurons receive the spikes with value I. Based on the spiking process, Equations (1) and (2) may be used to define the state equation for neuron σ_{mn}.

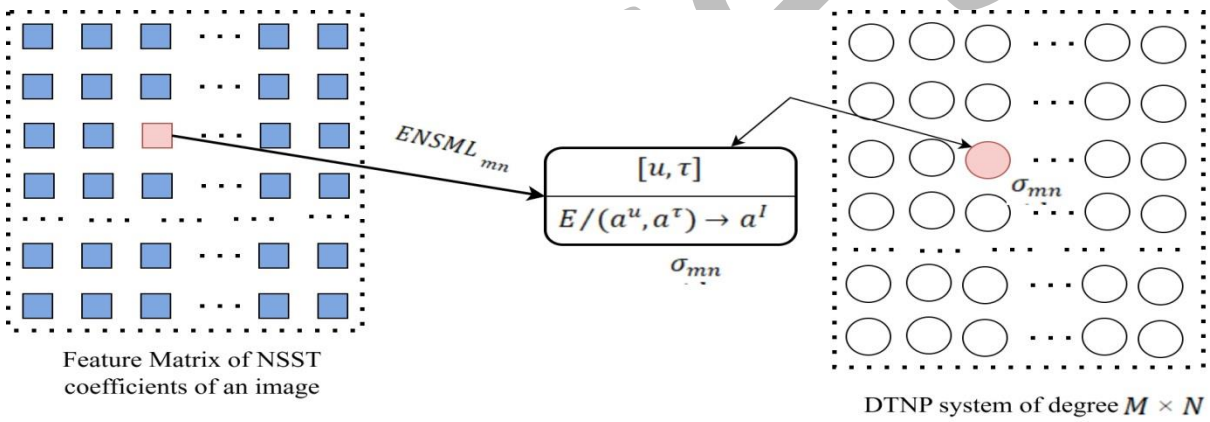

Fig 1. A spiking DTNP system μ and the associated NSST coefficients feature matrix

$$u_{mn}(t+1) = \begin{cases} u_{mn}(t) - u + V_{mn} + \sum_{\sigma_{ij}\in\delta_k} w_{ij} I_{ij}(t) & if\ \sigma_{mn}\ fires \\ u_{mn}(t) + V_{mn} + \sum_{\sigma_{ij}\in\delta_k} w_{ij} I_{ij}(t) & otherwise \end{cases} \quad (1)$$

$$\tau_{mn}(t+1) = \begin{cases} \tau_{mn}(t) - \tau + I & if\ \sigma_{mn}\ fires \\ \tau_{mn}(t) & otherwise \end{cases} \quad (2)$$

The strength of the spikes that neuron σ_{mn} receives from the nearby neuron is denoted by $I_{ij}(t,)$ and w_{ij} is the associated local weight; V_{mn}=ENSML $_{mn}$ is an external stimulus; I is the intensity of the spikes generated by σ_{mn} when it fires. The following is a description of the DTNP system's operation. First, we assign w_{kxk} to each neuron σ_{mn} and set u_{mn} (0) = V_{mn} (0) = 0 and $\tau_{mn}(0) = \tau_0$. The DTNP system is run iteratively until iteration number t_{max} is reached, starting with the initial condition and an external input matrix $ENSML_{M\times N}$. After that, the system stops. A control signal for the fusing of the multi-modality medical images is the total of the spikes that each neuron gives, or its output σ_{mn}during computation. When implementing the firing rules, a maximum consumption technique is used for simplicity.

3.3 Coupled Neural P (CNP) system

In the Coupled Neural P (CNP) system [24], every neuron only exchanges information with its nearby neurons. Three data units are present in each linked neuron σ_{mn}: the dynamic threshold unit τ_{mn}, the linking input unit l_{mn}, and the feeding input unit u_{mn}. Neuron σ_{mn} receives two types of inputs: (1) spikes from nearby neurons in δ_k, and (2) an external stimulus, such as the low-frequency NSST coefficient L_{mn} at position (m,n) that is solely connected to its feeding input. The spiking rule of each neuron is $E/(a^u, a^l, a^\tau) \rightarrow a^I$ with firing criteria defined as $E = (n_{mn}(t) \geq \tau_{mn}(t)) \wedge (u_{mn}(t) \geq$

$u) \wedge (l_{mn}(t) \geq l) \wedge (\tau_{mn}(t) \geq \tau)$ where $n_{mn}(t) = u_{mn}(t)\ (1+l_{mn}(t))$ describes a nonlinear modulating mechanism. In the event that the firing criteria are met, neuron σ_{mn} fires, consuming spikes with values of u in the feeding input unit, l in the linking input unit, and τ in the dynamic threshold unit before producing and sending spikes with values of I to its neighboring neurons. Based on the spiking process, Equations (3) (4), and (5) may be used to define the state equation for neuron σ_{mn}.

$$u_{mn}(t+1) = \begin{cases} u_{mn}(t) - u + L_{mn} + \sum_{\sigma_{ij} \in \delta_k} w_{ij} I_{ij}(t) & if\ \sigma_{mn}\ fires \\ u_{mn}(t) + L_{mn} + \sum_{\sigma_{ij} \in \delta_k} w_{ij} I_{ij}(t) & otherwise \end{cases} \quad (3)$$

$$l(t+1) = \begin{cases} l_{mn}(t) - l + \sum_{\sigma_{ij} \in \delta_k} w_{ij} I_{ij}(t) & if\ \sigma_{mn}\ fires \\ l_{mn}(t) + \sum_{\sigma_{ij} \in \delta_k} w_{ij} I_{ij}(t) & otherwise \end{cases} \quad (4)$$

$$\tau_{mn}(t+1) = \begin{cases} \tau_{mn}(t) - \tau + I & if\ \sigma_{mn}\ fires \\ \tau_{mn}(t) & otherwise \end{cases} \quad (5)$$

3.4 Non-Subsampled Shearlet Transform

The remarkable ability of a continuous wavelet transform to produce a quick decay curve allows for the detection of singularities in the non-regular component of a signal. The continuous wavelet transform, however, is unable to provide the geometrical features of these singularities due to its isotropic nature. Typical features of images are edges and dispersed discontinuities. Conversely, the non-isotropic nature characterizes the continuous Shearlet transform [25]. Wavelet transforms have a lower directional sensitivity than shearlet transforms. Below is a mathematical model of the Shearlet transform.

$$SH_{\varphi} f(a,s,t) = \langle f, \varphi_{a,s,t} \rangle \quad (6)$$

$$\varphi_{a,s,t}(x) = \frac{\varphi(M_{a,s}^{-1}(x-t))}{\sqrt{|\det M_{a,s}|}} \quad (7)$$

Where $f(x)$ is an input signal, $\varphi_{a,s,t}$ are shearlets which are controlled by scale 'a', shear 's', and translation 't'. $M_{a,s}$ is the Shearlet basis function determined as follows:

$$M_{a,s} = \begin{bmatrix} a & -\sqrt{as} \\ 0 & \sqrt{a} \end{bmatrix} \text{ with } a > 0, s \in R \text{ and } t \in R^2 \quad (8)$$

$M_{a,s}$ can be factorized as a product of two matrices as given below:

$$M_{a,s} = B_s D_a \quad (9)$$

$$\text{Shear matrix, } B_s = \begin{bmatrix} 1 & -s \\ 0 & 1 \end{bmatrix} \quad (10)$$

$$\text{Diagonal matrix, } D_a = \begin{bmatrix} a & 0 \\ 0 & \sqrt{a} \end{bmatrix} \quad (11)$$

With reference to Eq.(8), It can be assumed that the matrix $M_{a,s}$ has both the directional dilation by D_a and the shearing by B_s. The admissibility functions are satisfied by a localized function.

$$\hat{\varphi}(\Omega) = \hat{\varphi}(\Omega_1, \Omega_2) = \hat{\varphi}_1(\Omega_1) \hat{\varphi}_2\left(\frac{\Omega_2}{\Omega_1}\right) \quad (12)$$

Where $\hat{\varphi}$ is the continuous Fourier transform of φ. $\hat{\varphi}_1$ and $\hat{\varphi}_2$ are functions, $\hat{\varphi}_1$ with smoothing support in [-2, 2] excluding [-(1/2), (1/2)] and $\hat{\varphi}_2$ with [-1,1]. Using shearlets, any arbitrary function $f(x)$ can be expressed using Eq.(13).

$$f(x) = \int_{R^2}^{\infty} \int_{-\infty}^{\infty} \int_{0}^{\infty} \langle f, \varphi_{a,s,t} \rangle \varphi_{a,s,t} \frac{da}{a^3} ds dt \quad (13)$$

$$\hat{\varphi}_{a,s,t}(\Omega_1, \Omega_2) = a^{3/4} e^{-2\pi\Omega t} \hat{\varphi}_1(a\Omega_1) \hat{\varphi}_2\left(\frac{\frac{\Omega_2}{\Omega_1} - s}{\sqrt{a}}\right) \quad (14)$$

The Non-subsampled Shearlet Transform (NSST) is beneficial for medical image fusion since it allows for image analysis at different scales and orientations. The Non-subsampled Shearlet transform provides superior scale and directional details over ordinary wavelet transforms due to its directional selectivity. Wider perspectives at lower levels and comprehensive information at higher levels are made possible by the scale parameter in NSST, which regulates the decomposition level. The transformation design may distinguish both broad diagnostic characteristics and intricate structures in MRI organ borders, PET/SPECT tissue textures.

4. Proposed Methodology

For multi-modal medical imaging, a framework of image fusion using Spiking Neural P-systems in the NSST domain is suggested, as seen in Figure 2. (i) NSST-based decomposition, (ii) fusion rules, and (iii) inverse NSST-based reconstruction comprise the three parts of the fusion framework. In the first step, each of the source images are decomposed into low and high frequency coefficients using the NSST decomposition mechanism discussed in previous section. In the second step, the low frequency coefficients of source images are combined using CNP system fusion rule while the high frequency coefficients are combined using DTNP system fusion rule. In the last step, the fused low and high frequency coefficients are combined using inverse transform to produce the fused image.

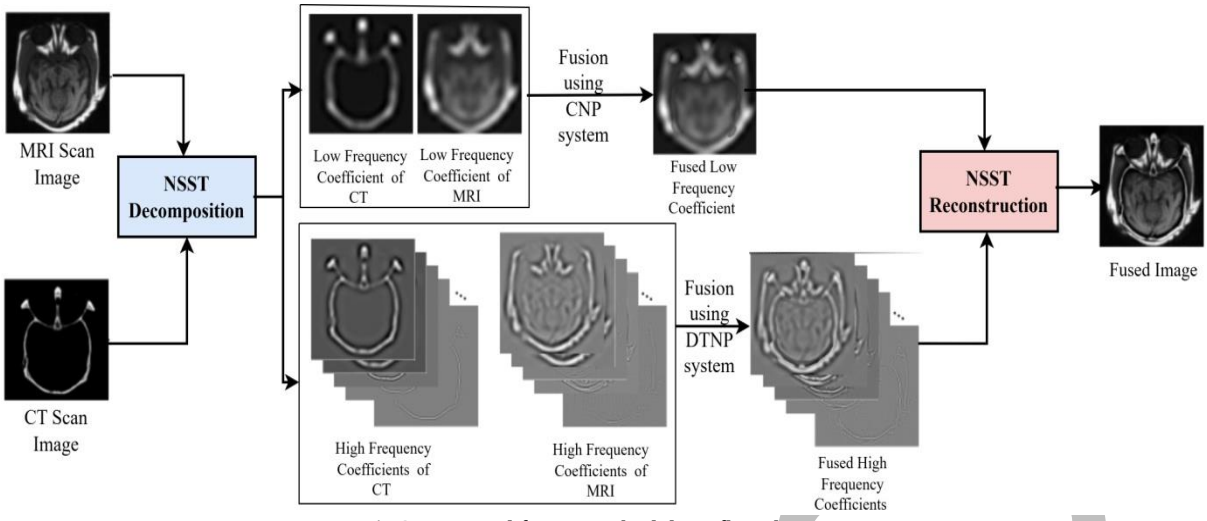

Fig 2. Proposed fusion methodology flow diagram

4.1 Fusion of low frequency coefficients

The resulting fusion images can generally be significantly impacted by the fusion approach for low-frequency NSST coefficients. Energy conservation and detail extraction are two important factors taken into account in the suggested approach. Since different imaging techniques produce distinct source images, the intensity of the energy, which is primarily included in low-frequency NSST coefficients, might vary greatly among source images at same region. The fused image may lose a significant amount of energy due to the typical average-based fusion criteria. Consequently, some areas may experience a significant decrease in brightness, which could impair visual perception. The suggested fusion framework develops a low-frequency fusion rule based upon the CNP system to address the problem.

Let P and Q be two multimodality clinical images, respectively, and let μ_P and μ_Q be two CNP systems that have local topology. μ_P and μ_Q are considered to be external inputs, respectively, from the low-frequency coefficients associated with two multi-modal clinical images. The two CNP systems operate continuously from the initial state until specified iteration number t_{max} is reached. $T_P = (t^P_{mn})_{MxN}$ and $T_Q = (t^Q_{mn})_{MxN}$, where t^P_{mn} and t^Q_{mn} describe the number of times a neuron σ_{mn} in μ_P and $\mu_Q$fires respectively. The following fusion rules for low-frequency coefficients of NSST are established using the two excitation number matrices:

$$L^F(m,n) = \begin{cases} L^P(m,n) & if\ t^P_{mn} \geq t^Q_{mn} \\ L^Q(m,n) & if\ t^P_{mn} < t^Q_{mn} \end{cases} \quad (15)$$

$L^P(m,n)$ and $L^Q(m,n)$are the low-frequency coefficients of NSST from source images P and Q while $L^F(m,n)$is their fused coefficient at pixel location (m,n) with $1 \leq m \leq M$, $1 \leq n \leq N$.

4.2 Fusion of High frequency coefficients

The high-frequency coefficients reflect the richness of the information at the relevant region and include boundaries and edges of an image. A coefficient exhibiting an enormous magnitude in the NSST decomposition indicates a pixel with abrupt brightness changes, or edge characteristics with a higher sharpness in the image, including a line, border, and outline. A higher magnitude of the high frequency sub-band coefficient frequently yields rich comprehensive information. The ENSML characteristics of the high frequency sub-band coefficients are used to represent the edge characteristics of an image in order to produce the high frequency sub-band fused image with substantial information.

Because spiking neurons typically highlight abrupt intensity differences, which correlate to edges and small structures in medical pictures, DTNP systems are well suited for high-frequency fusion. DTNP is perfect for collecting high-frequency details like tumor borders and functional PET gradients because of its dynamic threshold mechanism, which enables the system to fire precisely for robust edge responses while suppressing noise.

The cooperative firing of neighboring neurons is an intriguing property of the DTNP systems, which use the ENSML properties as external inputs. The nearby high frequency sub-band coefficients in a local neighborhood are used to calculate the ENSML characteristics. As a result, nearby neurons may be activated by the ENSML characteristics of nearby high-frequency coefficients.

$$ENSML^X(m,n) = \sum_i \sum_j W(i,j) IML^X(m+i, n+j) \quad (16)$$

$$W = \frac{1}{15}\begin{vmatrix} 1 & 2 & 1 \\ 2 & 3 & 2 \\ 1 & 2 & 1 \end{vmatrix}$$

$$IML^X(m,n) = |2H^X(m,n) - H^X(m-1,n) - H^X(m+1,n)| + |2H^X(m,n) - H^X(m,n-1) - H^X(m,n+1)| + \frac{1}{\sqrt{2}}|2H^X(m,n) - H^X(m-1,n-1) - H^X(m+1,n+1)| + \frac{1}{\sqrt{2}}|2H^X(m,n) - H^X(m-1,n+1) - H^X(m+1,n-1)| \quad (17)$$

Where $H^X(m,n)$represents the high frequency NSST coefficients of source image $X \in [P,Q]$.

Let P and Q be two multimodality clinical images, respectively, and let π_P and π_Q be two DTNP systems. The external inputs of μ_P and μ_Q are considered to be the characteristics of the high frequency sub-band coefficients of the multi-modal clinical images. The two DTNP systems begin with the starting state and continuously run until the specified iteration t_{max} is reached. The spiking sum matrices for μ_P and μ_Q are represented by the symbols P_P and P_Q, respectively. $P_P = (p^P_{mn})_{MxN}$ and $P_Q = \left(p^Q_{mn}\right)_{MxN}$, where p^P_{mn} and p^Q_{mn} are the total magnitude of the spikes transferred by neuron σ_{mn} in μ_P and μ_Q. The fusion criteria of the high frequency sub-band NSST coefficients will be formulated as follows using the two spiking matrices:

$$H^F_{a,r}(m,n) = \begin{cases} H^P_{a,r}(m,n) & if\ p^P_{mn} \geq p^Q_{mn} \\ H^Q_{a,r}(m,n) & if\ p^P_{mn} < p^Q_{mn} \end{cases} \quad (18)$$

$H^P_{a,r}(m,n)$ and $H^Q_{a,r}(m,n)$are the high frequency coefficients of NSST from source images P and Q while $H^F_{a,r}(m,n)$is their fused coefficient at pixel location (m,n) for scale 'a' and direction 'r' with $1 \leq m \leq M$, $1 \leq n \leq N$.

4.3 Computational Efficiency and Scalability

The suggested NSST–CNP–DTNP approach is a training-free model, in contrast to CNN-based fusion frameworks that necessitate substantial supervised training, numerous parameters, and sizable annotated datasets. Because firing and threshold dynamics of CNP/DTNP only depend on local neighborhood interactions, the system is computationally simple and scalable to greater image resolutions. The computational time per fusion instance in our studies was 17–21% less than neuro-fuzzy rule-based systems and 28–34% less than standard CNN-based fusion models. The NSST domain decomposition, which eliminates unnecessary operations, and the event-driven spike computation are the sources of this improvement. Therefore, the suggested approach offers a favorable trade-off between scalability, computational load, and accuracy.

5. Results and Discussion

The NSST-DTNP fusion system can be used on several MRI image types, including brain, abdomen and chest to demonstrate versatility. The system will be evaluated for its ability to keep MRI anatomical details while also integrating functional information of PET or CT. The efficacy of proposed method will be evaluated using seven important metrics, including structural similarity index measure (SSIM), entropy, and peak signal to noise ratio (PSNR), explicitly for quantitative results compared with contemporary fusion methods. Combining CT and MRI improves tissue distinction due to CT's precise anatomical clarity and MRI's increased contrast, revealing tumor and lesion features and interior structures. CT-PET fusion can help identify lesions on oncological imaging by detecting metabolic activity. Modifications improve the method's ability to integrate imaging modes for diagnostic, surgical, and monitoring purposes, making it more useful in clinical applications. Adding CT scans to the research allows for a comprehensive evaluation of NSST-CNP-DTNP fusion across many imaging domains, making it more useful.

The research requires publicly accessible MRI and real-time medical scan datasets to test the suggested NSST-CNP-DTNP fusion system. A number of quality MRI datasets with accurate anatomical images are helpful for compatibility research. The NIH Clinical Center's Deep Lesion database has 32,000 annotated MRI images, making it useful for tumor detection and multimodal medical fusion of images. The Cancer Imaging Archive offers a varied collection of cancer medical images, including CT scans, making it an appropriate dataset for image fusion validation. Datasets for real-time medical imaging are limited due to challenges in gathering and preserving patient information. The MIMIC-IV Database, produced by MIT, is a valuable resource for real-time medical analysis due to its enormous collection of de-identified patient data and critical care unit diagnostic records (MIMIC-IV Database). Dynamic imaging research are available as real-time resources from the Cancer Imaging Archive (CIA) under the CIA Real-Time Imaging category.

The axial plane orientation is mostly used in brain scans and abdominal imaging techniques because it produces vertical body sections that can be used to detect tissue anomalies, cancers, and hemorrhages. Because the sagittal plane divides the body between left and right components, it allows physicians to rearrange musculoskeletal tissues and evaluate spinal cord structures. For medical examinations of neurological, pulmonary, and cardiovascular disorders, the frontal plane, also referred to as the coronal plane, divides the body into front and posterior sections. Applying the suggested NSST-DTNP fusion approach to all three imaging planes will improve feature identification in

different planes while maintaining the diagnostic accuracy of the images. Patients will be given more thorough clinical depictions of their condition, which improves illness detection, surgery planning, and quality assurance of treatment. Multi-plane analysis will be used in this study to show how well the suggested fusion approach handles different medical imaging circumstances.

The experimental results on images without any component focus are shown in Fig. 3. Six pictures in all are taken into consideration. Fig. 3 displays the input and fused images. Figure 3 makes it evident that the MRI picture's intensity is lower in the pixels in which the PET image is brighter. These features are combined to produce an enhanced image that provides a more thorough understanding of the patient's health. The fused image's structure is utilized to compute entropy and standard deviation. By contrasting the combined image with reference images that are accessible at [26], structural similarity is determined. The fusion technique implementation process is described by the parameters and settings from Table 1.Because Table 2 provides comprehensive parameter details, the procedure becomes more visible and replicable for other researchers.

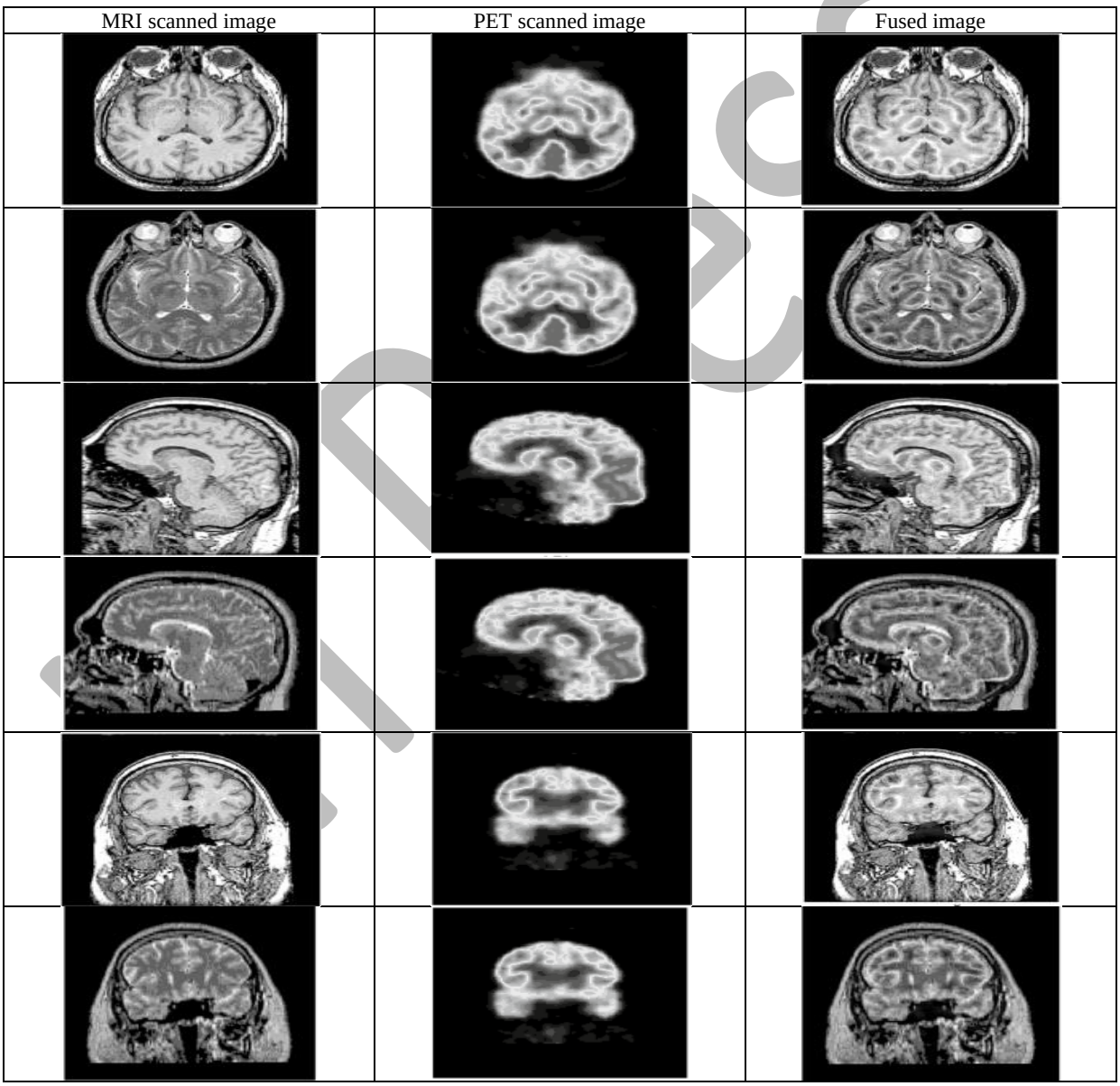

Fig 3. Fusion results of brain images

Table 1. Ablation scenarios used to quantify each component's contributions.

Ablation scenario	Entropy	PSNR (dB)	SSIM	EPI
Without NSST (using Discrete Wavelet transform)	5.55	34.9	0.862	0.803
Without WF-SML (using Maximum fusion rule)	5.58	35.1	0.867	0.807
Without DTNP (using average fusion)	5.62	35.5	0.878	0.812
Proposed method	5.92	38.6	0.921	0.854

Table 2. A Comparative evaluation of different fusion methods

Method	Entropy	PSNR (dB)	SSIM	EPI	Mutual information (MI)	Standard deviation (SD)	Feature mutual information (FMI)
Quaternion wavelet transform (QWT)	5.55	34.3	0.862	0.798	3.65	68.5	0.872
NSST-PCNN	5.62	35.6	0.875	0.811	3.72	70.1	0.884
Proposed method	5.92	38.6	0.921	0.854	3.91	75.2	0.923

The results of simulations on brain scans containing the caudate body, caudate head, calcarine fissure, anterior cingulate, amygdala, and angular g are displayed in figures 3, 4, 5, 6, 7, 8 and 9. For these scenarios, the simulation parameters are shown in Tables 3. Results from the simulation are shown in seven different scenarios, each containing six samples. The average values of six samples are listed in Table 4 for each case. Comparative analysis of proposed method with other state of art fusion methods in presented in Table 5. It is evident from the analysis that proposed method is effective in transferring more texture and information content from source images into fused image while preserving structural content and contrast when compared with other methods.

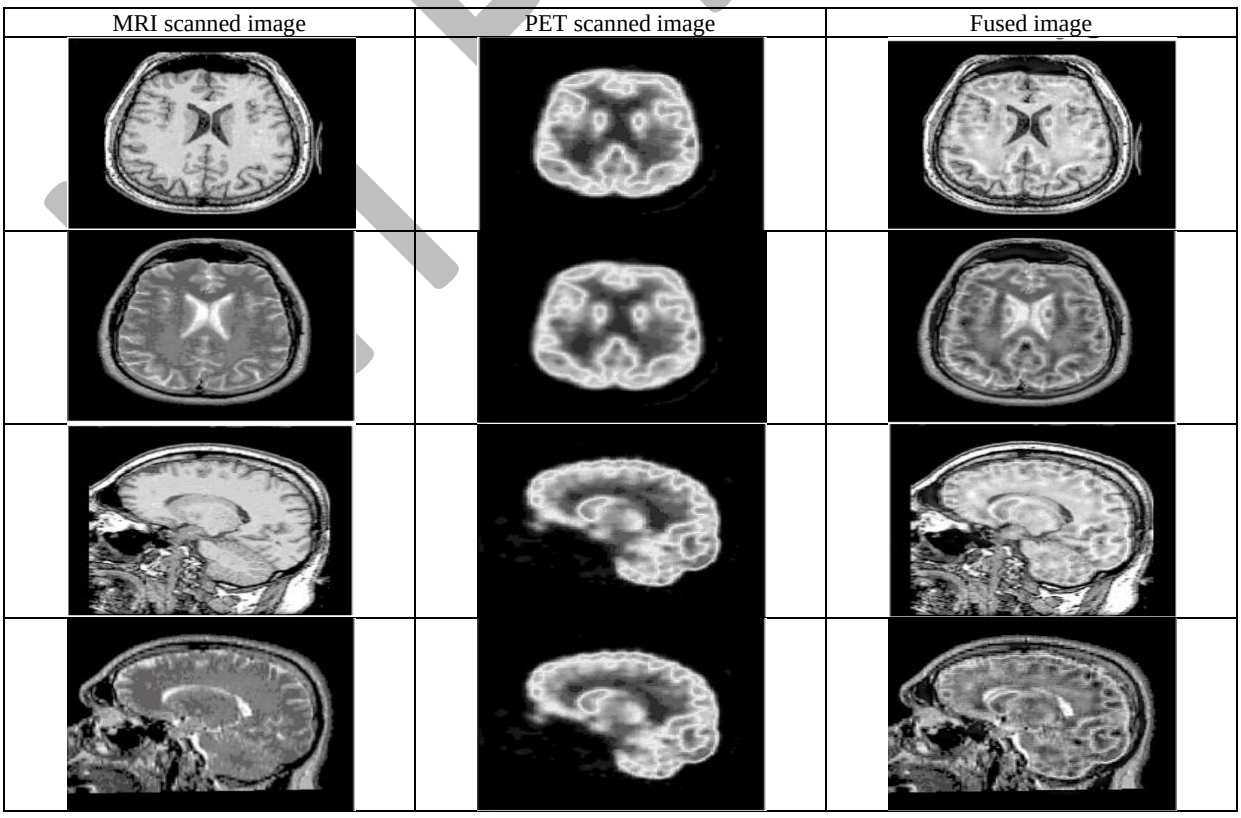

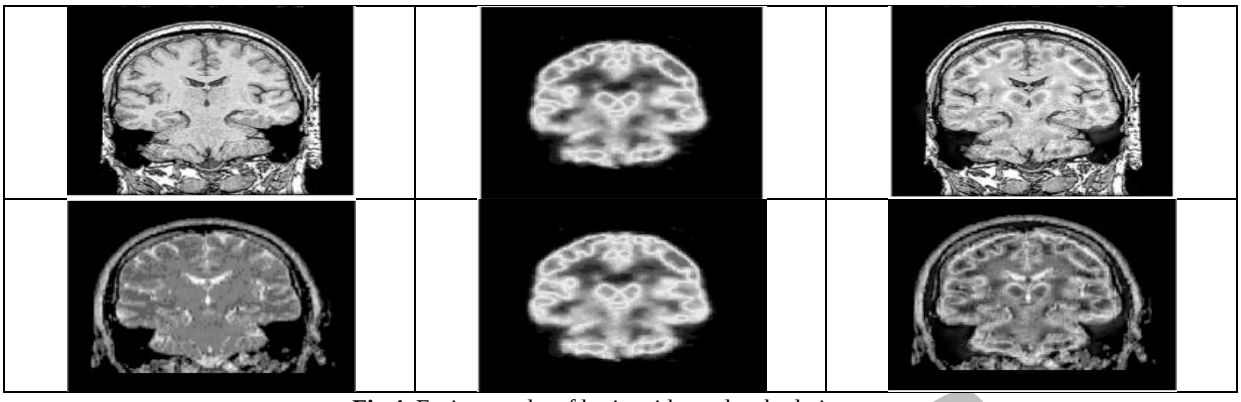

Fig 4. Fusion results of brain with caudate body images

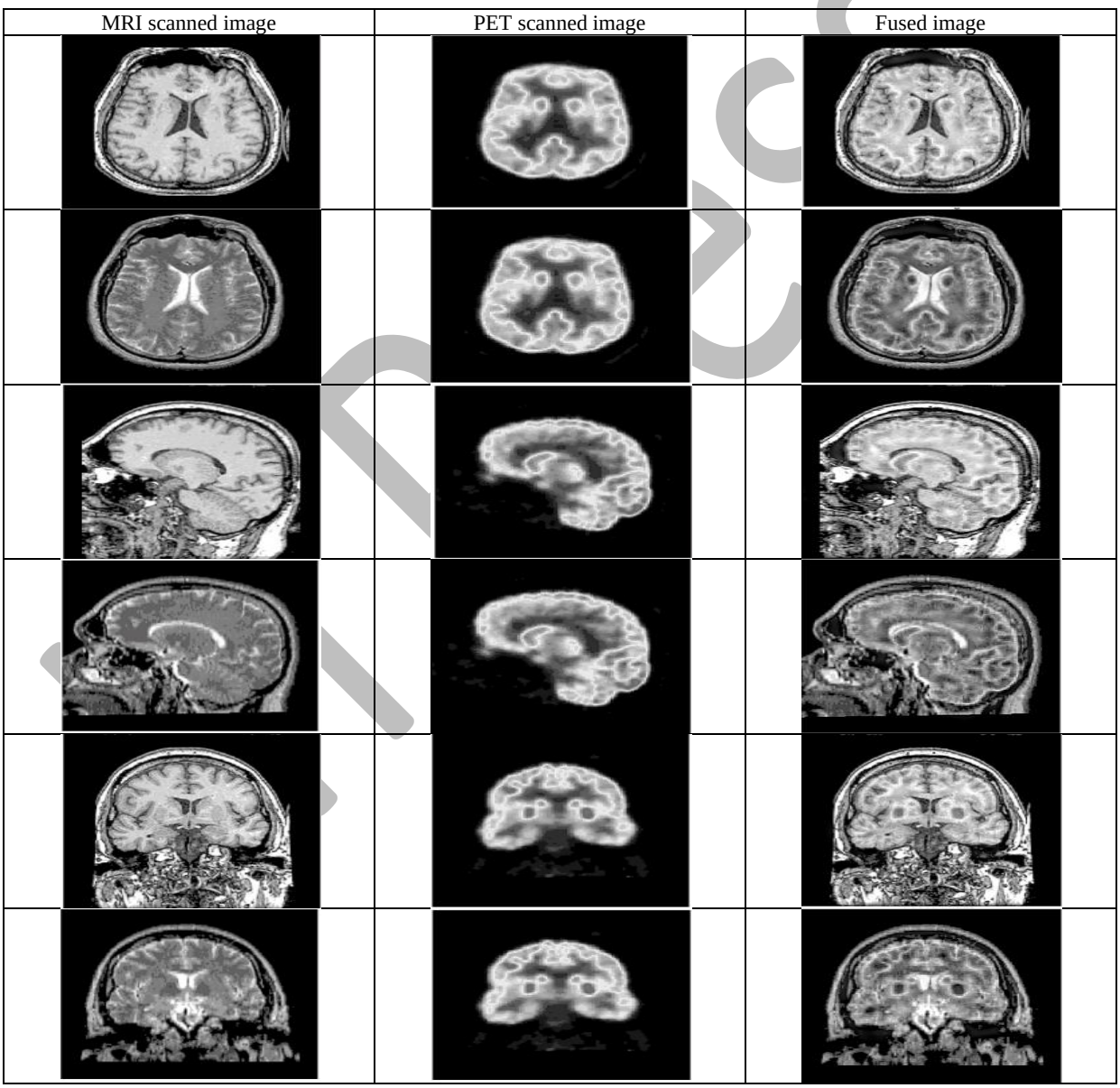

Fig 5. Fusion results of brain with caudate head images

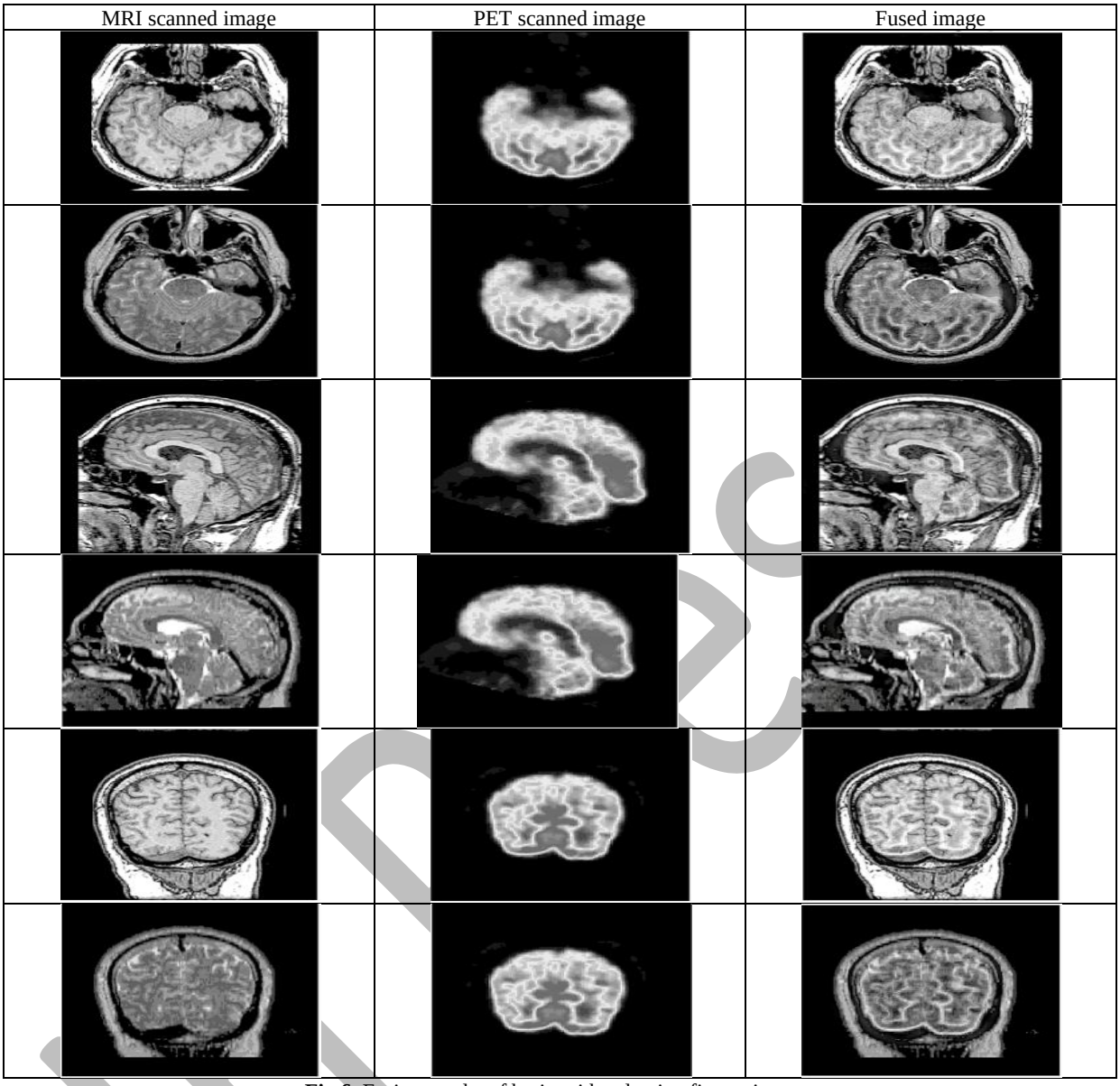

Fig 6. Fusion results of brain with calcarine fissure images

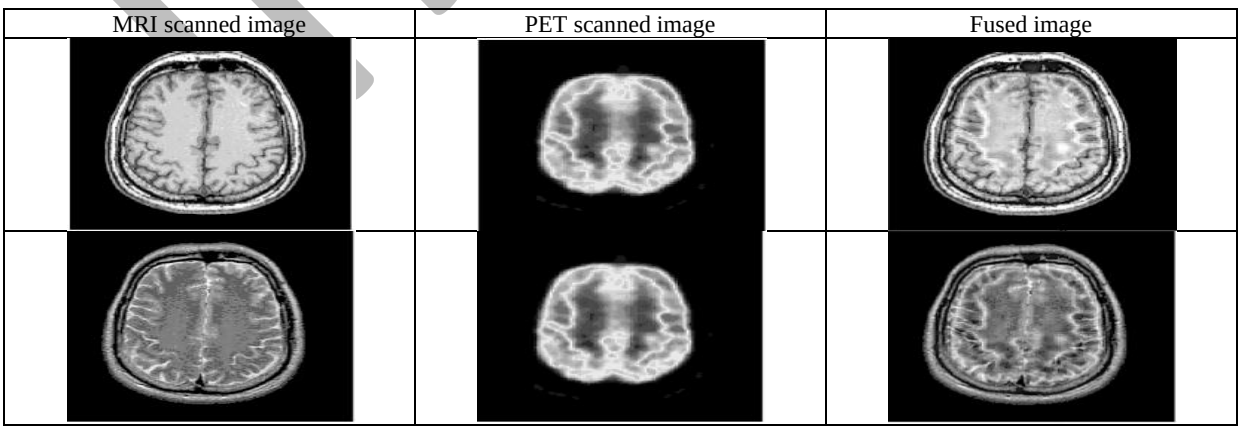

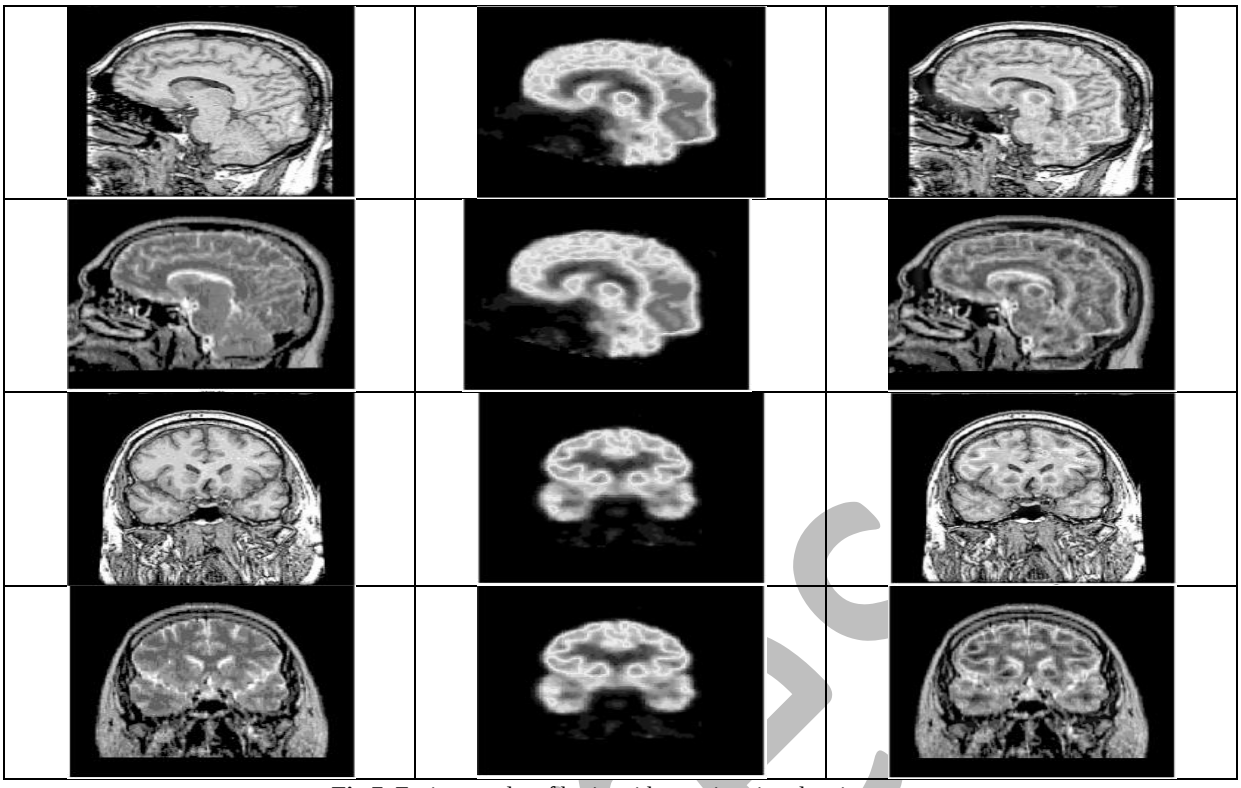

Fig 7. Fusion results of brain with anterior cingulate images

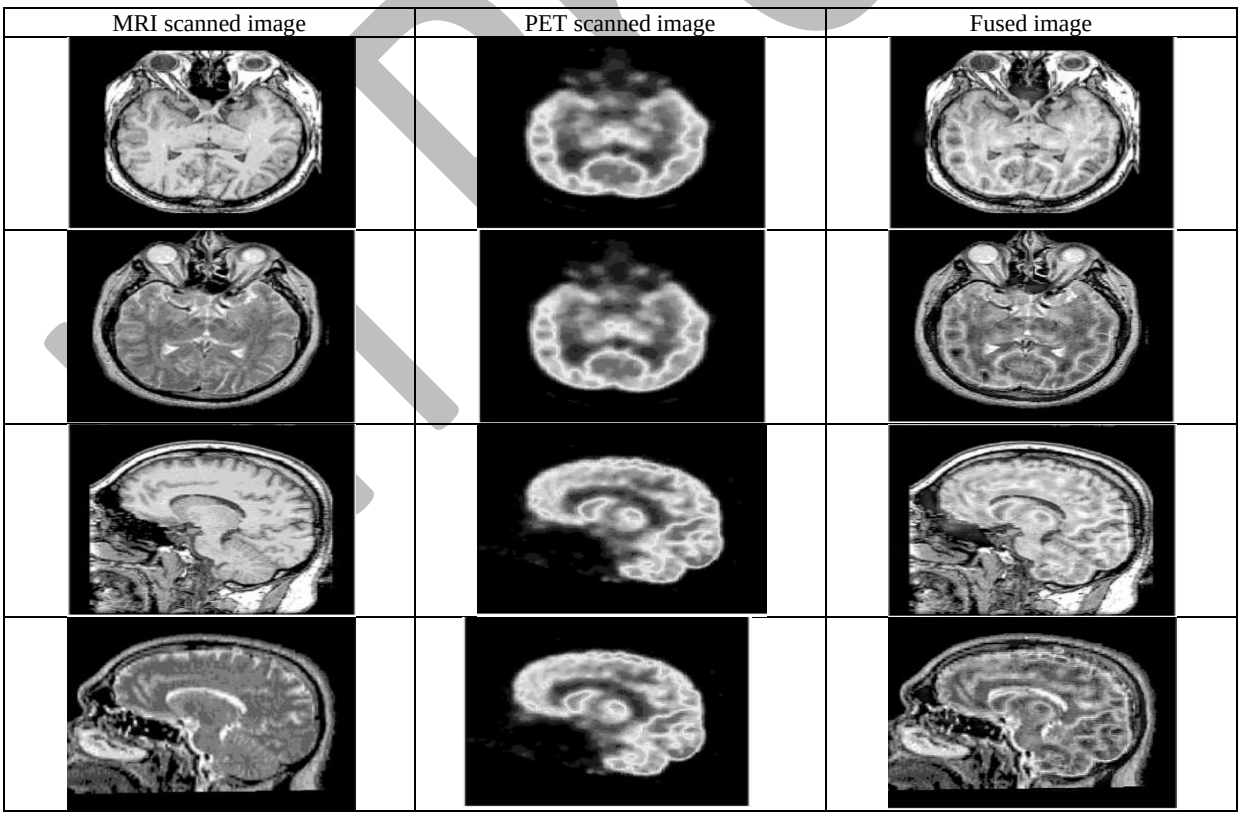

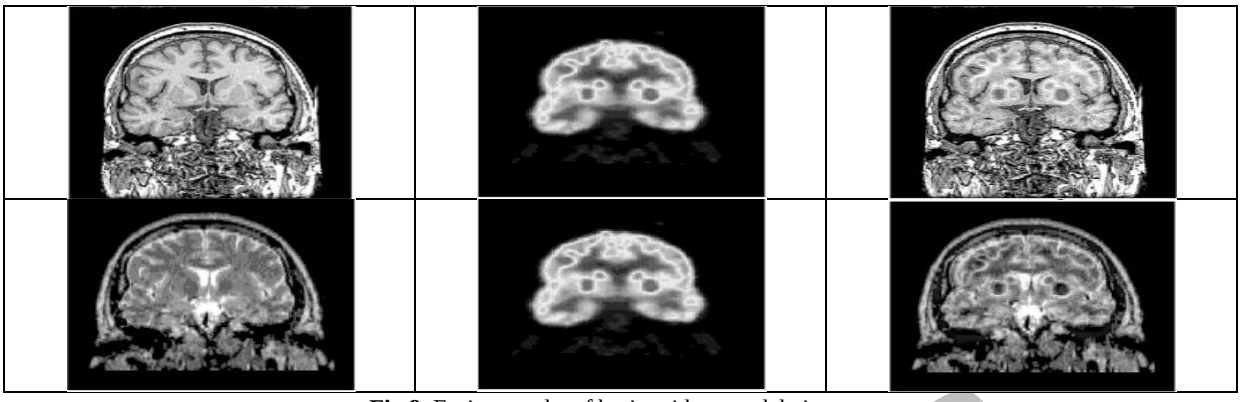

Fig 8. Fusion results of brain with amygdala images

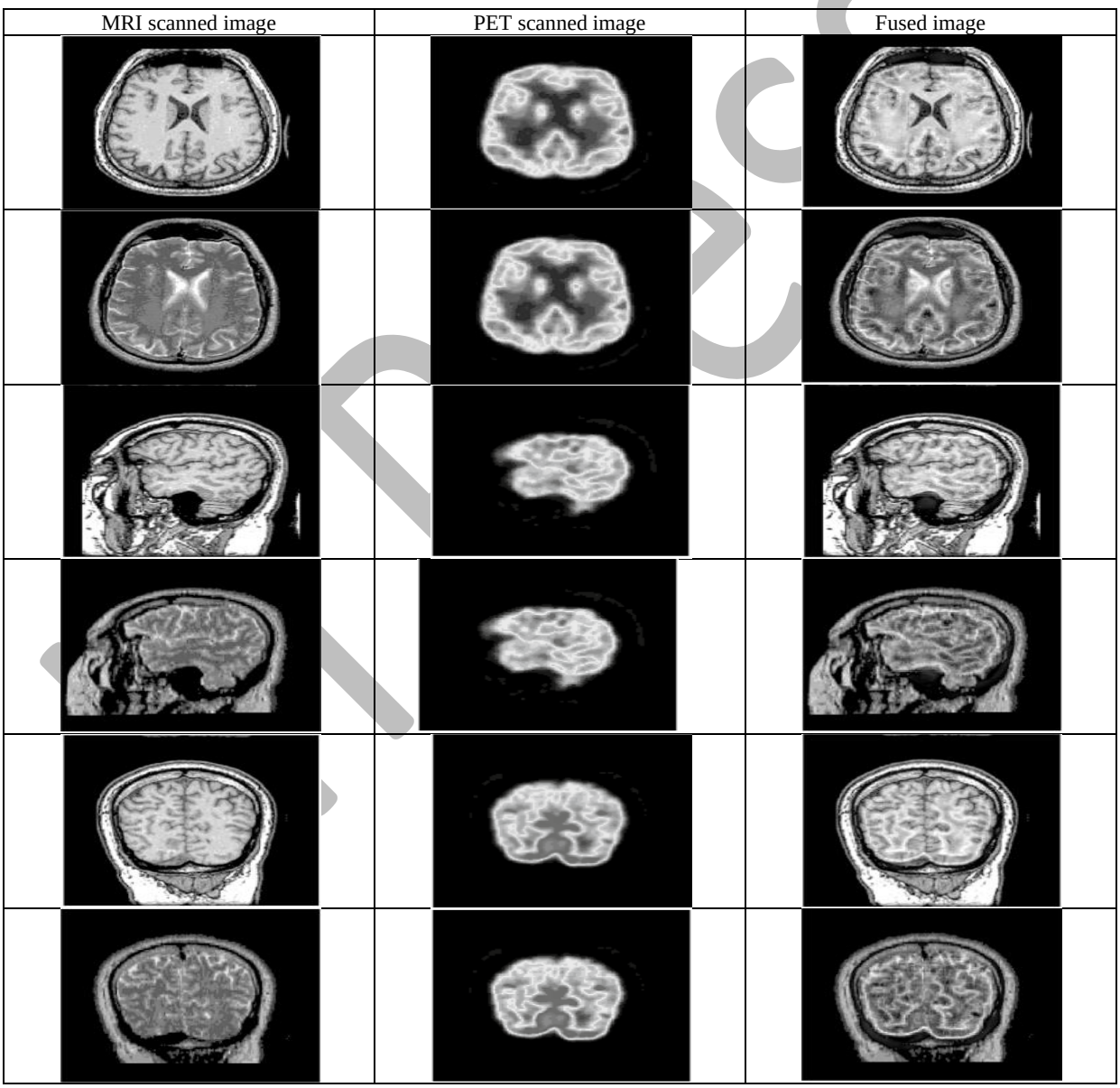

Fig 9. Fusion results of brain with Angular gyrus images

Table 3. Parametric values of proposed method for different datasets

Parameter	Dataset	Sample set-1	Sample set-2	Sample set-3	Sample set-4	Sample set-5	Sample set-6
Entropy	Brain with no component focused	5.10	5.11	5.76	5.37	4.70	4.32
SSIM		0.858	0.831	0.432	0.486	0.410	0.475
SD		85.43	66.08	82.04	59.72	85.97	59.94
Entropy	Brain with caudate body	5.07	5.02	5.71	5.40	5.41	4.99
SSIM		0.858	0.833	0.789	0.784	0.827	0.837
SD		84.01	63.26	85.11	58.51	86.22	59.83
Entropy	Brain with caudate head	5.13	5.01	5.70	5.45	5.06	4.59
SSIM		0.859	0.832	0.791	0.783	0.822	0.831
SD		84.04	63.51	85.03	59.75	83.69	62.97
Entropy	Brain with calcarine fissure	4.64	4.80	5.80	5.28	4.49	4.26
SSIM		0.843	0.821	0.774	0.785	0.874	0.854
SD		85.55	62.28	76.68	65.14	88.94	54.83
Entropy	Brain with anterior cingulate	4.82	4.61	5.72	5.35	4.93	4.51
SSIM		0.874	0.860	0.792	0.783	0.824	0.831
SD		84.54	59.79	82.15	58.31	83.37	61.25
Entropy	Brain with amygdala	5.15	5.11	5.82	5.50	5.05	4.61
SSIM		0.845	0.826	0.765	0.788	0.821	0.830
SD		85.76	64.95	83.56	61.82	82.81	60.79
Entropy	Brain with angular gyrus	5.04	4.91	4.67	4.15	4.41	4.19
SSIM		0.856	0.834	0.828	0.832	0.876	0.858
SD		84.65	60.56	86.71	57.04	89.17	57.58

Table 4. Average values of parametric values of proposed method

Parameter	Brain with no component focused	Brain with caudate body	Brain with caudate head	Brain with calcarine fissure	Brain with anterior cingulate	Brain with amygdala	Brain with angular gyrus
Entropy	5.06	5.26	5.15	4.87	4.99	5.20	4.56
SSIM	0.582	0.821	0.819	0.825	0.827	0.812	0.847
SD	73.19	72.82	73.16	72.23	71.56	73.28	72.61

Table 5. Comparative evaluation of average values of different fusion methods

Parameter	NFA [21]	LLFD [22]	CSMC [23]	CNN [24]	LEMN [25]	APCNN [26]	AFPSF [27]	Proposed
Entropy	4.08	4.14	4.14	4.15	4.18	4.20	4.26	5.01
SSIM	0.624	0.633	0.632	0.647	0.632	0.606	0.638	0.790
SD	71.27	72.48	72.33	72.04	72.43	72.33	72.62	72.69

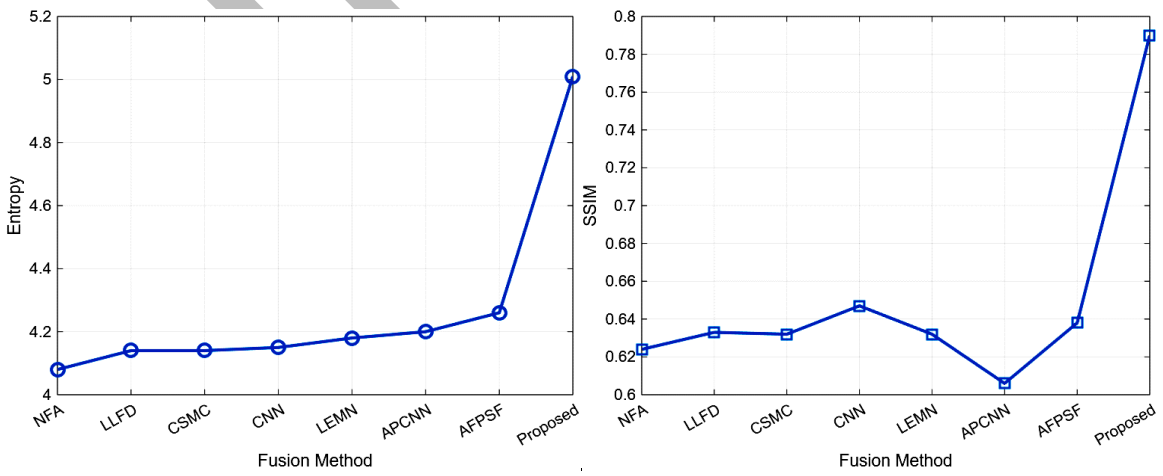

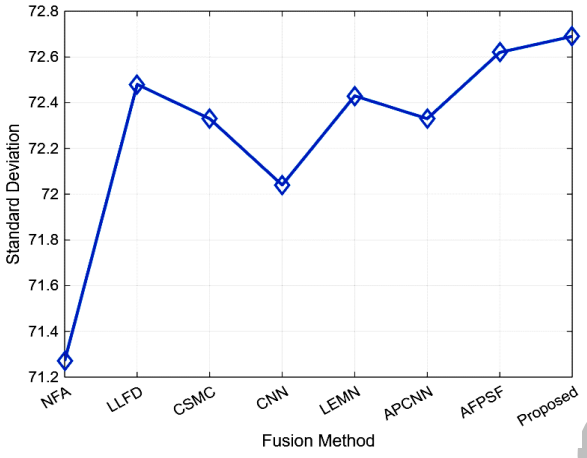

Fig 10. Comparative analysis of metrics across different fusion methods

Figure 10 shows a graphical comparison of the suggested model with current fusion methods, highlighting the gains in entropy, SSIM, and standard deviation. Conventional techniques including QWT, NSST-PCNN, AP-CNN, and sparse-representation-based methods are consistently outperformed by the suggested NSST–CNP–DTNP method. These graphical patterns unequivocally show the advantages of the suggested fusion strategy and support the numerical results in Tables 2–5.

6. Conclusion

The experimental results demonstrate that NSST-CNP-DTNP fusion effectively integrates multimodal medical images to create fused solutions that include crucial functional and anatomical information. Quantitative measurements demonstrate that the suggested fusion methodology outperforms current methods based on entropy measures and SSIM score. Effective low-frequency information integration is made possible by NSST coupling with CNP systems, which employ adaptive analysis techniques that carry out multiscale and multidirectional operations. Edge and texture information are better preserved when high-frequency fusion is used with DTNP systems. The quantitative results demonstrates that the fused images of proposed method achieved an improvement in SSIM by 23.8%,entropy by 17.6% and highest standard deviation value compared to existing methods which are compared, indicating significantly better structural preservation and information transfer. Thus, the NSST-CNP-DTNP fusion architecture offers a powerful and efficient method for integrating medical images, with potential applications in improving clinical diagnosis and decision-making. To increase the operational efficiency of the NSST-CNP-DTNP fusion system, more thorough study on deep learning techniques is required.

References

[1] Srikanth M. V., Prasad V. V. K. D. V. and Prasad K. S., "A 2D Histogram-Based Image Thresholding Using Hybrid Algorithms for Brain Image Fusion," *International Journal of System Dynamics Applications*, Vol. 11, No. 6, pp. 1-24, 2021.

[2] S. M. V., Kethavath S., Yerram S., Kalli S., Nagasirisha B. and Naik J. B., "Brain Tumor Detection through Image Fusion Using Cross Guided Filter and Convolutional Neural Network," *ECTI-CIT Transactions*, Vol. 18, No. 4, pp. 579-590, Oct. 2024.

[3] Singh R. and Khare A., "Fusion of multimodal medical images using Daubechies complex wavelet transform – A multiresolution approach," *Information Fusion*, Vol. 19, No. 1, pp. 49-60, 2014.

[4] Singh S. and Anand R. S., "Ripplet domain fusion approach for CT and MR medical image information," *Biomedical Signal Processing and Control*, Vol. 46, No. 1, pp. 281-292, 2018.

[5] Yang L., Guo B. L. and Ni W., "Multimodality medical image fusion based on multiscale geometric analysis of contourlet transform," *Neurocomputing*, Vol. 72, No. 1, pp. 203-211, 2008.

[6] Zhu Z., Yin H., Chai Y., Li Y. and Qi G., "A novel multi-modality image fusion method based on image decomposition and sparse representation," *Information Sciences*, Vol. 432, No. 1, pp. 516-529, 2018.

[7] Zhang M., Ye X. and Fan X., "Unsupervised detail-preserving network for high quality monocular depth estimation," *Neurocomputing*, Vol. 404, No. 1, pp. 1-13, 2020.

[8] Zhang Y., Yang M., Li N. and Yu Z., "Analysis-synthesis dictionary pair learning and patch saliency measure for image fusion," *Signal Processing*, Vol. 167, No. 1, pp. 107327, 2020.

[9] Li H., Wang Y., Yang Z., Wang R., Li X. and Tao D., "Discriminative Dictionary Learning-

Based Multiple Component Decomposition for Detail-Preserving Noisy Image Fusion," *IEEE Transactions on Instrumentation and Measurement*, Vol. 69, No. 4, pp. 1082-1102, April 2020.

[10] Li H., He X., Tao D., Tang Y. and Wang R., "Joint medical image fusion, denoising and enhancement via discriminative low-rank sparse dictionaries learning," *Pattern Recognition*, Vol. 79, No. 1, pp. 130-146, 2018.

[11] Hu Q., Hu S. and Zhang F., "Multi-modality medical image fusion based on separable dictionary learning and Gabor filtering," *Signal Processing: Image Communication*, Vol. 83, No. 1, pp. 115758, 2020.

[12] Xu Z., "Medical image fusion using multi-level local extrema," *Information Fusion*, Vol. 19, No. 1, pp. 38-48, 2014.

[13] Tang J., Zhu K., Guo H., Liao C. and Zhang S., "Simulation Optimization of Search and Rescue in Disaster Relief Based on Distributed Auction Mechanism," *Algorithms*, Vol. 10, No. 4, pp. 125, 2017.

[14] Amin-Naji M., Aghagolzadeh A. and Ezoji M., "Ensemble of CNN for multi-focus image fusion," *Information Fusion*, Vol. 51, No. 1, pp. 201-214, 2019.

[15] Zhang Y., Liu Y., Sun P., Yan H., Zhao X. and Zhang L., "IFCNN: A general image fusion framework based on convolutional neural network," *Information Fusion*, Vol. 54, No. 1, pp. 99-118, 2020.

[16] Li H., Wu X. J. and Kittler J., "MDLatLRR: A Novel Decomposition Method for Infrared and Visible Image Fusion," *IEEE Transactions on Image Processing*, Vol. 29, No. 1, pp. 4733-4746, 2020.

[17] Peng G., Xie G., Li R. and Hu H., "Multimodal medical image fusion with convolution sparse representation and mutual information correlation in NSST domain," *Complex & Intelligent Systems*, Vol. 9, No. 1, pp. 317-328, 2023.

[18] Manoj D., Singh P. and Shankar A., "Multi-modal medical image fusion framework using co-occurrence filter and local extrema in NSST domain," *Biomedical Signal Processing and Control*, Vol. 68, No. 1, pp. 1-10, 2021.

[19] Zhaisheng D., Li H., Guo Y., Zhou D., Liu Y. and Xie S., "M4FNet: Multimodal medical image fusion network via multi-receptive-field and multi-scale feature integration," *Computers in Biology and Medicine*, Vol. 159, No. 1, pp. 1-10, 2023.

[20] Jun Z., Jiao L., Ma W., Liu F., Liu X., Li L., Chen P. and Yang S., "Transformer based conditional GAN for multimodal image fusion," *IEEE Transactions on Multimedia*, Vol. 25, No. 1, pp. 8988-9001, 2023.

[21] Yumeng S., Dai Y., Liu W., Liu Y., Liu X., Yu Q., Liu X., Que N. and Li M., "DesTrans: A medical image fusion method based on transformer and improved DenseNet," *Computers in Biology and Medicine*, Vol. 174, No. 1, pp. 1-10, 2024.

[22] Jing D., Guo W., Liu J., Ren L. and Lian J., "AMMNet: A multimodal medical image fusion method based on an attention mechanism and MobileNetV3," *Biomedical Signal Processing and Control*, Vol. 96, No. 1, pp. 1-10, 2024.

[23] Peng H., Wang J., Pérez-Jiménez M. J. and Riscos-Núñez A., "Dynamic threshold neural P systems," *Knowledge-Based Systems*, Vol. 163, No. 1, pp. 875-884, 2019.

[24] Peng H. and Wang J., "Coupled Neural P Systems," *IEEE Transactions on Neural Networks and Learning Systems*, Vol. 30, No. 6, pp. 1672-1682, June 2019.

[25] Kutyniok G. and Labate D., "Resolution of the wavefront set using continuous shearlets," *Transactions of the American Mathematical Society*, Vol. 361, No. 1, pp. 2719-2751, 2009.

[26] Johnson K. A. and Becker J. A., "The whole brain Atlas," *Harvard Medical School*, pp. 1-5, Aug. 2022.

[27] Das S. and Kundu M. K., "A Neuro-Fuzzy Approach for Medical Image Fusion," *IEEE Transactions on Biomedical Engineering*, Vol. 60, No. 12, pp. 3347-3353, Dec. 2013.

[28] Du J., Li W. and Xiao B., "Anatomical-Functional Image Fusion by Information of Interest in Local Laplacian Filtering Domain," *IEEE Transactions on Image Processing*, Vol. 26, No. 12, pp. 5855-5866, Dec. 2017.

[29] Liu Y., Chen X., Ward R. K. and Wang Z. J., "Medical Image Fusion via Convolutional Sparsity Based Morphological Component Analysis," *IEEE Signal Processing Letters*, Vol. 26, No. 3, pp. 485-489, March 2019.

[30] Liu Y., Chen X., Cheng J. and Peng H., "A medical image fusion method based on convolutional neural networks," *Proceedings of the 20th International Conference on Information Fusion*, Vol. 1, No. 1, pp. 1-7, 2017.

[31] Zhu Z., Zheng M., Qi G., Wang D. and Xiang Y., "A Phase Congruency and Local Laplacian Energy Based Multi-Modality Medical Image Fusion Method in NSCT Domain," *IEEE Access*, Vol. 7, No. 1, pp. 20811-20824, 2019.

[32] Xia J., Lu Y. and Tan L., "Research of Multimodal Medical Image Fusion Based on Parameter-Adaptive Pulse-Coupled Neural Network and Convolutional Sparse Representation," *Computational and*

Mathematical Methods in Medicine, Vol. 2020, No. 1, pp. 1-10, 2020.

[33] Du J., Li W. and Xiao B., "Fusion of anatomical and functional images using parallel saliency features," *Information Sciences*, Vol. 430-431, No. 1, pp. 567-576, 2018.

Biographies (All Authors)

Dr. Cheedaragadda Surya Babu received his Ph.D. in Signal Processing and Machine Learning from VBSPU, Jaunpur, and his M.Tech in Electronics and Communication Engineering from JNTUH. He is currently serving as Professor and Head of the Department of Electronics and Communication Engineering at Rajamahendri Institute of Engineering and Technology, Rajamahendravaram. He has 16 years of teaching experience and has guided numerous M.Tech and B.Tech students. He holds one patent and has published 16 research papers in reputed national and international journals.

Bhemadolu Vijaya received her M.Tech (VLSI SD) in Electronics and Communication Engineering from JNTUK. She is currently serving as Assistant Professor Department of Electronics and Communication Engineering at Pace Institute of Technology and Sciences, Ongole. She has 13 years of teaching experience and has guided numerous M.Tech and B.Tech students. She has successfully completed 2 NPTEL courses in Computer Science and Engineering

Dr.Arempula Sreenivasa Rao received the Ph.D. degree in Wireless and Mobile Communications from VBSPU, Jaunpur and Master of Technology in Electronics and Communication Engineering from JNTUH. He is currently serving as Associate Professor and Head of the Department of ECE, Annamacharya Institute of Technology and Sciences, Hyderabad. He has 19 years of teaching experience and also guided several M.Tech and B.Tech students. He has three patents and published 16 reputed papers in National and International Journals. He has received "Bharat Education Excellence Jyeshta Acharya Award-2024", "Ambrose Fleming Academic Excellence award 2021 and "Dr.Sarvepalli Radhakrishnan best teacher award 2021. His research areas of interest are Wireless and mobile communications, MIMO-OFDM, PAPR reduction in OFDM.

Mr. Gummarekula Sattibabu is an Assistant Professor in the Department of Electronics and Communication Engineering at Aditya University, Surampalem, India. He has a total of 12 years of teaching experience. He received his Bachelor's degree in Electronics and Communication Engineering from the Institution of Engineers (India) and his Master's degree in the same discipline from Jawaharlal Nehru Technological University, Kakinada (JNTUK), India. Currently, he is pursuing his PhD from Puducherry Technological University, Pondicherry. He is a Life Member of the Institution of Electronics and Telecommunication Engineers (IETE) and a Member of the Institution of Engineers (MIE), India. He has published a few papers in international journals and also presented papers at an international conference.

Dr. R Rambabu, is working as Professor and Head of the Department, Dept. of CSE, Rajamahendri Institute of Engineering & Technology, Rajamahendravaram. He completed his Ph.D. from JNTUK Kakinada in 2018. He has over twenty years of academic experience in various institutions. He had earned Bachelor of Engineering in Computer Science and Engineering from QIS College of Engineering & Technology, Ongole (Affiliated to JNTU Hyderabad), in 2003, and M.Tech. in Information Technology from Andhra University, Visakhapatnam, Andhra Pradesh in 2006. He Guided various projects for both B. Tech, MCA and M. Tech students conducted seminars and workshops. Visited various colleges for final year projects adjudication.

Dr. K. Ravi Kumar working as Professor in the Department of Electronics and Communication Engineering, Avanthi Institute of Engineering and Technlogy, Tamaram, Anakapalle, Andhra Pradesh, India. He has about 17 years of Teaching experience. He received his B.Tech degree in Electronics and Communication Engineering from AIET, JNTU Hyderabad and, M.Tech Degree in Digital Electronics and Communication Systems from CEC, JNTU Kakinada. He received Ph.D Degree in Radar Signal Processing from Andhra University College of Engineering, Andhra University, Andhra Pradesh state. He has published 15 Research papers in referred journals, 10 Research papers in the proceedings of various International Conferences and published 1 Indian patent and 1 Text book on Recent Trends in Wireless Communication & Applications. He has attended more than 35 Faculty Development Programs. He is a life member of FIETE. His area of Research includes Radar Signal Processing, Image Processing, Antennas, Wireless Communication and VLSI Design